Life-Cycle of Structures and Infrastructure Systems – Biondini & Frangopol (Eds)

The effect of road roughness on vehicle-bridge interaction modeling

A. Aloisio & R. Alaggio
University of L'Aquila, L'Aquila, Italy

A. Contento & B. Briseghella
Fuzhou University, Fuzhou, China

ABSTRACT: The study of the bridge response under moving loads is commonly investigated with two alternative approaches. One approach represents the vehicle as a moving load, the other with sprung mass models. This study is aimed to compare the two approaches and evaluate the difference in their accuracy to assess if there are cases where vehicle bridge-interaction modelling (i.e. the use of sprung mass models) is needed to accurately estimate the bridge response. For this purpose, both a moving load model and a one degree of freedom sprung mass model have been implemented and used to compare the bridge response under different road roughness. The probabilistic distributions of two indicators, used to compare the bridge displacement responses in three roughness scenarios with variable velocity and different vehicle mass and dynamics, are derived through Montecarlo simulations. It is found that an increasing level of road roughness modelled according to ISO-8608 increases the differences between the predictions of the models.

1 INTRODUCTION

Vehicle-bridge interaction (VBI) problems were extensively studied for several reasons that include the growing interest in the safety assessment of infrastructures. Additionally, the interest in vibration-based approaches for structural health monitoring (SHM) of infrastructures further fed the research in VBI modelling.

Additionally VBI models can be either coupled or uncoupled. In the coupled models, the moving vehicle contributes to the bridge vibration, whereas in the uncoupled models vehicle dynamics does not affect the bridge response. Uncouples models are often preferred due to their relatively simple implementation, reduced computational cost, and robustness against numerical instability. However, the assumptions of the uncoupled approach cannot always be acceptable. In many cases the accurate modelling of VBI is essential for precisely predicting fatigue phenomena occurring when a structure is subjected to repeated load cycles, like bridges under vehicular traffic. The accurate prediction of of the fatigue life is fundamental for the structure's life-cycle assessment (LCA). Thus, VBI modelling is necessary component of the mathematical framework needed for the LCA of infrastructure.

To the authors' knowledge, a few papers are attempting to understand the trade-off between model complexity and accuracy in VBI problems (González et al., 2022). Additionally, several investigations lack experimental validation and focus on the modal parameters, i.e. estimating the time-variance of the bridge response in terms of instantaneous frequency, damping and mode shape. Experimental investigations are generally based on time-frequency analyses using vibration data in terms of velocity or acceleration (Li et al., 2022; Quqa et al., 2022). Recently, Gonzalez (González et al., 2022) attempted to quantify the modelling error in predicting the bridge response under moving vehicles using uncoupled methods. However, his attempt lacks experimental validation and focuses on a few scenarios.

Within this framework, this paper's ultimate goal is to clarify when the assumptions of the uncoupled model are reasonable or not and to highlights the role of road roughness in the differences between the two approaches. For this purpose, the authors used a moving load

DOI: 10.1201/9781003323020-334

model and a one degree of freedom sprung mass model to simulate the bridge response under the effect of a running vehicle and performed Montecarlo simulations varying three parameters describing the vehicle dynamics (velocity, mass and natural frequency) and the roughness level according to the ISO:8608. The outcomes of the analyses lead to a probabilistic model to describe the difference between the two modelling approaches. Since the accuracy of the two models depends on the quantity being predicted (e.g. use the midspan deflection to estimate the maximum load effect and the time-history of a dynamic system), the authors select two discrepancy indicators (i.e. error estimates): the relative variation in the maximum deflection and (ii) the modal assurance criterion. The former is relevant for safety problems, where the primary intent is to assess the maximum load effect on the structure. The latter is essential for those researches where the bridge time-history is involved in the analyses. The elements of novelty can be summarised in

1. estimating the error gap between coupled and uncoupled approaches using mathematical models validated against experimental results;
2. developing a computationally efficient Finite-Difference (FD) formulation of the VBI problem;
3. fitting the discrepancy indicators with suitable probability density functions that can be used to estimate the modelling error when using concentrated load models.

2 VEHICLE-BRIDGE INTERACTION MODEL

The randomness of the road surface roughness can be represented with a periodic modulated random process. In ISO-8608 (ISO/TC et al., 1995) specifications, road surface roughness and vehicle speed are related through the relation between velocity power spectral density (PSD) and displacement PSD. The general expression for the displacement PSD of the road surface roughness is $S_d(n) = S_d(n_0) \cdot (n/n_0)^{-a}$, where n_0 = 0.1 cycles/m is the reference spatial frequency, a is an exponent of the PSD, and n is the spatial frequency (cycles/m). The classification of the road roughness is based on a constant vehicle velocity PSD by taking a = 2. The road roughness profile can be generated through the following equation:

$$r(x) = \sum_{i=1}^{Q} d_i \cos(n_i x + \Theta_i). \tag{1}$$

In the equation, n_i is the i-th spatial frequency, Θ_i is the random phase angle, and d_i is the i-th amplitude computed as $d_i = \sqrt{2S_d(n)\Delta n}$ with Δn denoting the sampling interval of the spatial frequency.

The dynamic equilibrium equation of the vehicle mass m_v can be written as follows:

$$m_v(\ddot{w}_v + \ddot{r} + \ddot{w}_b) + c\dot{w}_v + k_v w_v = 0, \tag{2}$$

where m_v, c_v, and k_v are respectively the sprung mass, the damping coefficient, and the stiffness of the vehicle. The absolute displacement of the vehicle mass is written as the summation of three terms: w_v, r, and w_b. Namely, w_v indicates the relative displacement between the road surface and the center of gravity of the vehicle mass, r indicates the road roughness, and w_b is the beam deflection measured from the line axis of the bridge. The contact force due to the vehicle oscillation f_c does not include the weight of the sprung-mass system and can be written as

$$m_w(\ddot{r} + \ddot{w}_b) + f_c - c_v\dot{w}_v - k_v w_v = 0, \tag{3}$$

where m_w is the mass of the wheel.

The bridge can be described as an Euler-Bernoulli beam. The EB beam has a constant mass per unit length $\rho_c A_c$ (where ρ_c is the specific mass of concrete and A_c is the cross-section area of the beam) and Ac constant flexural rigidity $E_c I_c$ (where E_c is the Young's modulus of concrete and I_c the cross-section inertia of the beam). The vertical displacement $w_b(x, t)$ of the bridge is governed by the following partial differential equation (Frỳba, 2013):

$$\rho_c A_c \ddot{w}_b(x,t) + E_c I_c w_{r,xxxx}(x,t) = \delta(x-ct)(f_c + m_w g + m_v g) \tag{4}$$

where δ is the Dirac delta. The left and right boundary conditions for a pinned-pinned beam are

$$\text{Left}: \quad w_b(0,t) = 0 \;\; w_{b,xx}(0,t) = 0; \quad \text{Right}: \quad w_b(L,t) = 0 \;\; w_{b,xx}(L,t) = 0. \tag{5}$$

The VBI equations (Equations 2 and 4) can be written in matrix form by discretizing the beam into n elements with a Δx length. The spatial discretization is obtained using the finite difference method that leads to the following coupled system of equations:

$$\begin{aligned} &\begin{bmatrix} \rho_c A_c \Delta x \boldsymbol{I} + m_w \delta \otimes \delta^{\boldsymbol{T}} & \boldsymbol{0} \\ m_v \delta^T & m_v \end{bmatrix} \begin{Bmatrix} \ddot{\boldsymbol{w}}_b(t) \\ \ddot{w}_v(t) \end{Bmatrix} + \begin{bmatrix} E_c I_c \boldsymbol{D}_4 & -\delta k_v \\ 0 & k_v \end{bmatrix} \begin{Bmatrix} \boldsymbol{w}_b(t) \\ w_v(t) \end{Bmatrix} + \\ &+ \begin{bmatrix} \boldsymbol{C} & -\delta c_v \\ \boldsymbol{0} & c_v \end{bmatrix} \begin{Bmatrix} \dot{\boldsymbol{w}}_b(t) \\ \dot{w}_v(t) \end{Bmatrix} + \begin{Bmatrix} \delta[-m_v g + m_w(\ddot{r} - g)] \\ m_v \ddot{r}(t) \end{Bmatrix} = 0. \end{aligned} \tag{6}$$

In Equation 6, $\boldsymbol{I}$ and $\boldsymbol{0}$ are the identity and null matrices, respectively, and $\boldsymbol{D}_4^{\{n \times n\}}$ is the approximate fourth matrix derivative. Additionally, $\boldsymbol{\delta}$ is the discretization of the Dirac function, $\boldsymbol{w}_b(t)$ collects the vertical deflection of the bridge discretized in N segments, and $\boldsymbol{C}_r$ is the damping matrix. The damping matrix is estimated using the Rayleigh approximation and is assumed proportional to the mass and stiffness matrices following the Rayleigh approach (Chopra, 1975). The i-th term of the discretized Dirac function (δ_i) is

$$\delta_i = \begin{cases} 1, & \text{if } \; i = \left[\frac{ct}{\Delta x} + 0.5\right] \wedge i = 1 \\ \frac{|ct - i\Delta x|}{\Delta x}, & \text{if } \; i = \left[\frac{ct}{\Delta x} + 0.5\right] \wedge i > 1 \\ 1 - \frac{|ct - i\Delta x|}{\Delta x}, & \text{if } \; i = \left[\frac{ct}{\Delta x} + 0.5\right] - 1 \wedge i > 1 \\ 0, & \text{else} \end{cases}, \tag{7}$$

where $[\cdot]$ denotes the rounding function. Equation 6 can be solved using the Dormand-Prince method based on an explicit Runge-Kutta temporal discretization (Dormand and Prince, 1980).

3 EXPERIMENTAL TESTS AND MODEL CALIBRATION

The bridge span under investigation belongs to the Italian motorway network. It is a simply-supported, prestressed concrete girder. The girder has the trapezoidal cross-section shown in Figure 1. The cross-section is 2.3m high, with two cantilevered wings 3.85m wide, and pre-stressed by bonded post-tensioned tendons. A pair of piers, whose centre distance is about 40m, sustains each bridge span.

3.1 *Experimental setups*

The response of the considered bridge span is measured in terms of acceleration and displacement of the mid-span. The setup for the accelerations consists in two rows of seven equally-spaced Force Balance Accelerometers (FBA); the experimental equipment for the displacements consists of an easel supporting a laser sensor. The dynamic tests are carried out under the excitation of a moving two-axes vehicle with mass 3860kg (Jin et al., 2022).The modal parameters are estimated using the covariance-driven Stochastic Subspace Identification (SSI) method (Peeters and De Roeck, 2001). For each setup, the data are sampled at a 200Hz rate and used for SSI and subsequent modal analysis to derive eigenfrequencies, damping ratios, mode shapes, covariances of the modal parameters, and, as a consequence, the bending stiffness of the beam model.

3.2 *Model calibration*

In the analysis, the vehicle velocity and its characteristic in terms of mass and stiffness are assumed known, as well as the area of the cross section A_c, the weight per unit of volume of

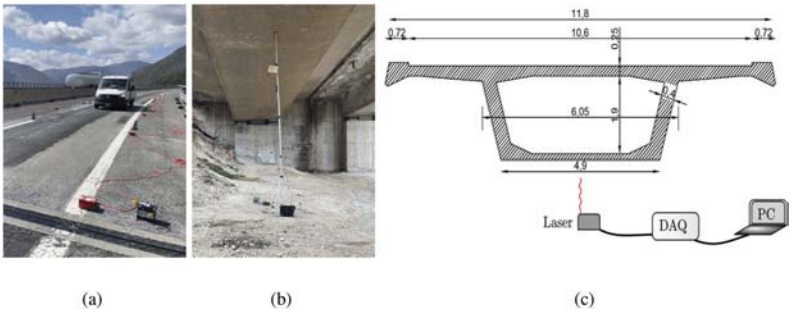

Figure 1. (a) View of the bridge with the accelerometers, view (b) and scheme (c) of the experimental setup.

concrete ρ_c, and the natural frequency of the first bending mode, estimated from output-only dynamic identification, are also used as input parameter to further constraint the optimization problem. The bridge spatial discretization is assumed equal to 0.2m, approximately equal to the wheel footprint, while the sampling frequency equal to 100Hz. The remaining unknown parameters of the VBI model are the bending stiffness *EI*, the equivalent viscous damping of the bridge ξ_b, and the roughness level $S_d(n_0)$. The viscous damping is included in the VBI model optimization because its dynamic identification could be unreliable due to its possible underestimation (Frizzarin et al., 2010). The authors follow a three-step approach for estimating the three unknown parameters:

1. the bending stiffness (*EI*) is estimated from the first bending mode of the considered bridge span;
2. the bridge damping (ξ_b) is estimated from experimental displacement response using the VBI model without road roughness;
3. the bridge roughness ($S_d(n_0)$) is estimated from experimental displacement response using the VBI model with road roughness.

The first mode closely resembles that of a pinned-pinned beam.Such bending mode can be reasonably used (in terms of mode shapes and natural frequencies) to estimate the bending stiffness *EI* of an equivalent beam model. To estimate *EI*, the authors solve a nonlinear least-squares problem (He et al., 2021) that which leads to find a global minimum of the objective function for $E \approx 1.575\text{Nm}^2$.

Conversely, the experimental displacement data are used to calibrate the bridge damping and the road roughness. The calibration is performed by using a genetic optimization algorithm (Sirotti et al., 2021). The genetic algorithm performs iteration of parameters with the goal of minimizing the integral of the difference between experimental and simulated displacement. As anticipated, the authors assume the value of the bending stiffness *EI* to further constrain the optimization problem that provided $\xi_b = 0.02$ and $S_d(n_0) = 2 \cdot 10^{-5}$ as optimum values of the parameters. The damping value is consistent with that of concrete structures, while the roughness level corresponds to a profile class A, according to the ISO:8608 classification.

Figure 2 plots the experimental displacement response of the bridge span against the predictions of the moving load (labelled load-smooth) and VBI models (labelled mass-smooth).The experimental data refer to the transit of a two-axes vehicle with a 3860kg mass, moving at constant velocity approximately equal to 80km/h. Such data reveal a significant noise level. However, the maximum beam deflection is low, and close to the sensor resolution ($\approx 10^{-2}$mm). The maximum deflection is approximately equal to 0.08mm. The model predictions are in good agreement with the experimental data, especially in the first part of the response and after the vehicle has crossed the bridge. Two significant aspects arise from the observation of Figure 2:

- in case of no or negligible roughness, there is no substantial difference between the VBI and moving load models. Therefore, the two responses are almost indistinguishable.
- even a minor level of road roughness (road profile A) leads to differences between the two models because the road roughness activates a VBI phenomenon, which is evident in the second part of the transit (shaded red rectangle). The VBI model (in red) can closely

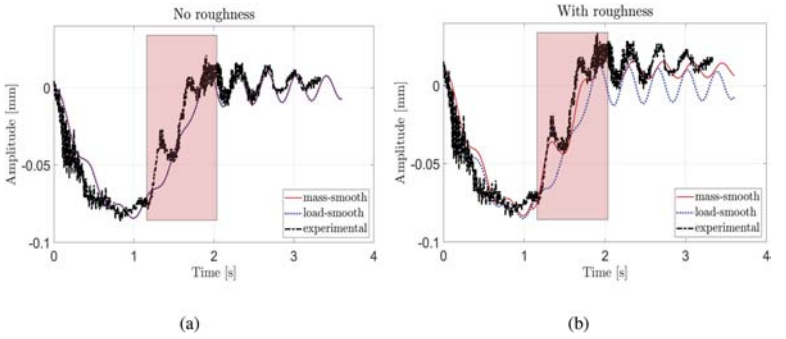

Figure 2. Experimental validation of the VBI and the concentrated force models in case of constant velocity (a) without and (b) with roughness ($S_d(n_0) = 2 \cdot 10^{-5}$).

follow the experimental data, especially the peaks arising in this part of the response. Conversely, the moving load model is not significantly influenced by the road roughness. The two models do not lead to noteworthy differences in maximum deflections, but the difference manifests as additional peaks due to the vehicle dynamics.

4 PARAMETRIC ANALYSES AND DISCREPANCY INDICATORS

A parametric analysis is performed to assess how the vehicle dynamics affects the bridge response under different roughness conditions. The parameters varied in the analyses are the vehicle velocity c, in the range 50–150 [km/h], the vehicle mass m_v, in the range 1–50 [ton], and the viscous damping coefficient of the vehicle, in the range 0.15–0.30. Such ranges reasonably represent the variation related to the variability of the vehicular traffic. Additionally, the values of $S_d(n_0)$ for the considered road roughness profiles according to ISO 8608 are $S_d(n_0) = 16 \cdot 10^{-6}\text{m}^3$/cycle for Profile Class A, $S_d(n_0) = 64 \cdot 10^{-6}\text{m}^3$/cycle for Profile Class B, and $S_d(n_0) = 256 \cdot 10^{-6}\text{m}^3$/cycle for Profile Class C. The three-dimensional parameters' space is sampled following the Latin hypercube sampling scheme (Iman and Conover, 1979). The number of samples is set equal to 10000, which allowed to obtain a value of the COV (< 0.1%) . The authors used two discrepancy indicators to quantify the differences between the two predictions, one referred to the maximum displacement and the other to the cross-correlation, following the definition of the modal assurance criterion. Such indicators read

$$\delta = \frac{\max(|\boldsymbol{w}_{vbi}|) - \max(|\boldsymbol{w}_{cl}|)}{\max(|\boldsymbol{w}_{cl}|)}; \text{MAC} = \frac{\left|\boldsymbol{w}_{vbi} \cdot \boldsymbol{w}_{cl}^T\right|^2}{\left(\boldsymbol{w}_{vbi} \cdot \boldsymbol{w}_{vbi}^T\right)\left(\boldsymbol{w}_{cl} \cdot \boldsymbol{w}_{cl}^T\right)}; \tag{8}$$

where $\boldsymbol{w}_{vbi}$ and $\boldsymbol{w}_{vbi}$ collect the bridge responses from the VBI and concentrated load models. Given the roughness level, the road roughness is randomnly varied in each run of the two models.

The results of the parametric analyses in terms of δ and MAC are first used to estimate the Sobol sensitivity indexes (Sobol, 1993).

Table 1. Sobol sensitivity indicators for the effects of weight, damping, and velocity of the vehicle.

	δ	MAC	δ	MAC	δ	MAC
Parameter	Class A		Class B		Class C	
Weight	0.53	0.67	0.63	0.57	0.50	0.49
Damping	0.25	0.25	0.26	0.27	0.23	0.44
Velocity	0.21	0.24	0.30	0.28	0.42	0.45

Table 1 shows the Sobol sensitivity indicators, which estimate the effects of the weight, damping, and velocity of the vehicle on δ and MAC for the three roughness classes. The weight has a dominant effect on values of δ and MAC obtained for the three road classes (> 50%),

whereas, the effects of damping, and velocity are almost equal and range between 20 and 30%. Increments in the road roughness, from class A to C, cause an increment in the effects of damping and velocity on the chosen discrepancy indicators.

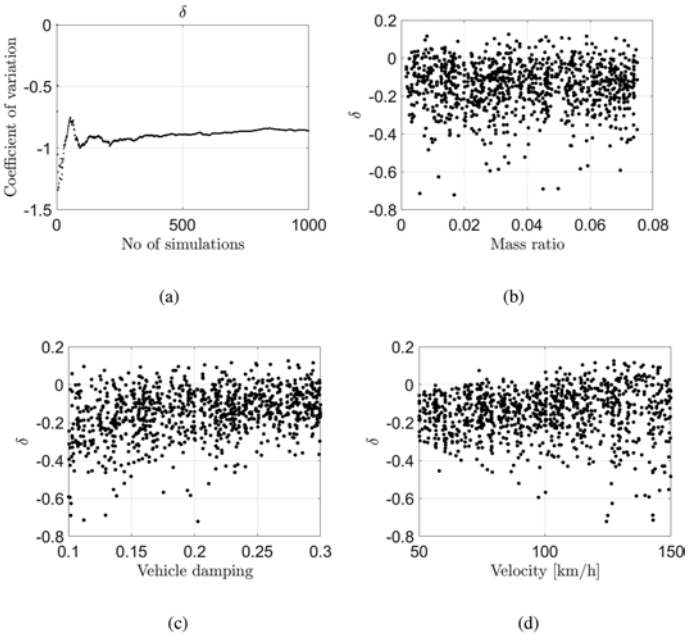

Figure 3. (a) Coefficient pf variation of δ (Equation 8) as a function of the number of simulations. (b)-(d) Comparison between coupled and uncoupled models in terms of δ in Equation 8 as a function of the mass ratio, vehicle damping, velocity given a roughness class A.

Figure 2 shows the plots of δ as a function of the mass ratio (vehicle mass divided by the bridge mass), velocity and damping of the vehicle. Using these results the authorsderived the probability density functions of the δ and MAC parameters as functions of the mass, damping, and velocity of the vehicle.

5 PROBABILISTIC DENSITY FUNCTIONS OF THE DISCREPANCY INDICATORS

The parameters δ and MAC obtained from the parametric analyses (Table 2) are fitted by suitable probability density functions. Specifically, it is assumed that

$$Z_i = T(Y_i) \sim N\left(\mu_i, \sigma_i^2\right), \tag{9}$$

where $T(.)$ is the two-parameters Box-Cox transformation, Y_i $\{\delta$,MAC$\}$ are random variable associated to two parameters, and μ_i, and σ_i^2, are unknown parameters (i = $\{\delta$, MAC$\}$). The posterior distribution of the parameters $\boldsymbol{\Theta} = \{\mu_i, \sigma_i\}$ is derived by means of the Bayes' rule in closed form assuming a prior of the joint distribution of μ_i and σ_i^2 in the form $p(\boldsymbol{\Theta}) \propto 1 \cdot \sigma_i^{-2}$. The two posterior marginal distributions are a t distribution for μ_i

$$\mu_i \sim t\left(\overline{z_i}, s_i^2/n, n-1\right), \tag{10}$$

and an Inverse-Gamma distribution for σ^2

$$\sigma^2 \sim IG\left((n-1)/2, s_i^2(n-1)/2\right). \tag{11}$$

In Equations (10) and (11), $\overline{z_i}$ is the mean value of the realizations of the transformed random variables, s_i is the correspondent corrected sample standard deviation, and $n = 1000$ is the number of realizations of z_i. The values of $\overline{z_i}$ and s^2 for the δ and MAC indicators related to each roughness class can be found in Table 5.

Table 2. Posterior statistics of the fitting probability density functions δ.

Roughness class	Descriptive parameter	λ_1	λ_2	Sample mean $\tilde{z}_i$	Sample standard deviation s_i
A	δ	1.800	0.722	-0.344	0.006
	MAC	3.400	0.0	-0.057	0.001
B	δ	1.800	1.459	0.110	0.059
	MAC	1.700	0.000	-0.202	0.009
C	δ	1.800	3.086	1.780	0.607
	MAC	1.700	0.000	-0.622	0.065

6 ANALYSIS OF THE RESULTS

Figure 4 shows the histogram plots of the δ and MAC functions. The road roughness plays a crucial role in magnifying the VBI effects because it activates the vehicle dynamics, which interacts with the bridge significantly, especially for frequency ratios close to 1. Consequently, an increase in road roughness entails increasing the difference between the VBI and moving load models. The moving load model is not conservative: the percentage of underestimation of the beam deflection rises from nearly 14% to almost 90% as the road roughness increases from Class A to Class C. Such results shows that there are cases, and in particular those with high road roughness, where the effects of VBI cannot be neglected. Consequently, to use moving load models, which are usually easier to implement, it is necessary to separately account for the additional effect of VBI that can be estimated using the fitted probability density functions of δ.

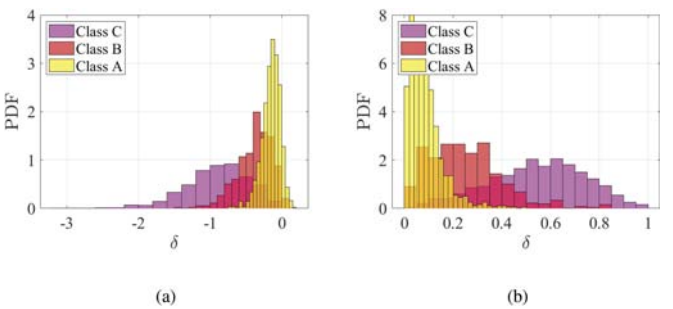

Figure 4. Histograms of δ and 1-MAC for the considered roughness classes.

In mid-span bridges, like the one considered in this paper, especially those belonging to high-level road networks, the road roughness belongs to class A and the increase of deflection due to VBI is, on average, 14%. In design, the potential underestimation of the load effects due to moving load models is compensated by including safety factors and load values corresponding to high fractiles of given probability distributions according to national and international standards.

7 CONCLUSIONS

This paper quantifies the effect of road roughness on vehicle bridge interaction (VBI) in a mid-span prestressed concrete bridge response. The bridge is modelled as a pinned-pinned Euler

Bernoulli beam, while two vehicle models are compared to simulate the vehicle transit: a concentrated load and a sprung-mass model. The first model does not include the mutual interaction between the bridge and the vehicle dynamic. It is used as a reference model to estimate the modelling error related to the lack of VBI effects. The differences between the two models are quantified in terms of relative error (δ) and correlation (MAC) between time histories. The governing equations are solved numerically after temporal and spatial discretization. It is found that the roughness triggers VBI phenomena and leads to higher discrepancies between the VBI and load models. Averagely, the load model underestimates the load effect by 14%, 37% and 90% in roughness classes A, B, and C, respectively. Future research papers will extend this study to different bridge typologies by varying the frequency ratio, i.e. the ratio between the vehicle and bridge natural frequency and more detailed VBI models. Additionally, the authors will extend the analyses further to include the effect of roughness in VBI due to vehicle braking.

REFERENCES

Aloisio, A., Pasca, D. P., Alaggio, R., and Fragiacomo, M. (2020). Bayesian estimate of the elastic modulus of concrete box girders from dynamic identification: A statistical framework for the a24 motorway in italy. *Structure and Infrastructure Engineering*, pages 1–13.

Chopra, A. K. (1975). Dynamics of structures.

Dormand, J. R. and Prince, P. J. (1980). A family of embedded runge-kutta formulae. *Journal of computational and applied mathematics*, 6(1):19–26.

Frizzarin, M., Feng, M. Q., Franchetti, P., Soyoz, S., and Modena, C. (2010). Damage detection based on damping analysis of ambient vibration data. *Structural Control and Health Monitoring*, 17(4):368–385.

Fryba, L. (2013). *Vibration of solids and structures under moving loads*, volume 1. Springer Science & Business Media.

González, A., Covián, E., and Casero, M. (2022). Verifying the suitability of uncoupled numerical methods for solving vehicle-bridge interaction problems. *Structure and Infrastructure Engineering*, pages 1–18.

He, L., Castoro, C., Aloisio, A., Zhang, Z., Marano, G. C., Gregori, A., Deng, C., and Briseghella, B. (2021). Dynamic assessment, fe modelling and parametric updating of a butterfly-arch stress-ribbon pedestrian bridge. *Structure and Infrastructure Engineering*, pages 1–12.

Iman, R. L. and Conover, W. J. (1979). The use of the rank transform in regression. *Technometrics*, 21 (4):499–509.

ISO/TC, T. C., Vibration, M., Measurement, S. S. S., of Mechanical Vibration, E., and as Applied to Machines, S. (1995). *Mechanical Vibration–Road Surface Profiles–Reporting of Measured Data*, volume 8608. International Organization for Standardization.

Jin, N., Dertimanis, V. K., Chatzi, E. N., Dimitrakopoulos, E. G., and Katafygiotis, L. S. (2022). Subspace identification of bridge dynamics via traversing vehicle measurements. *Journal of Sound and Vibration*, page 116690.

Li, H., Wang, T., and Wu, G. (2022). A bayesian deep learning approach for random vibration analysis of bridges subjected to vehicle dynamic interaction. *Mechanical Systems and Signal Processing*, 170:108799.

Lotfi, B. and Huang, L. (2016). An approach for velocity and position estimation through acceleration measurements. *Measurement*, 90:242–249.

Peeters, B. and De Roeck, G. (2001). Stochastic system identification for operational modal analysis: a review. *Journal of Dynamic Systems, Measurement, and Control*, 123(4):659–667.

Quqa, S., Giordano, P. F., and Limongelli, M. P. (2022). Shared micromobility-driven modal identification of urban bridges. *Automation in Construction*, 134:104048.

Sirotti, S., Pelliciari, M., Di Trapani, F., Briseghella, B., Carlo Marano, G., Nuti, C., and Tarantino, A. M. (2021). Development and validation of new bouc–wen data-driven hysteresis model for masonry infilled rc frames. *Journal of Engineering Mechanics*, 147(11):04021092.

Skolnik, D. A. and Wallace, J. W. (2010). Critical assessment of interstory drift measurements. *Journal of structural engineering*, 136(12):1574–1584.

Sobol, I. M. (1993). Sensitivity estimates for nonlinear mathematical models. *Mathematical modelling and computational experiments*, 1(4):407–414.